Late Holocene sea-cliff retreat recorded by 10Be profiles across a coastal platform: Theory and example from the English Channel

Vincent Regard, Thomas Dewez, D.L. Bourles, H. Anderson, Anne Duperret, Stéphane Costa, Laëtitia Leanni, Eric Lasseur, Kevin Pedoja, Grégoire M. Maillet

Late Holocene sea-cliff retreat recorded by ^{10}Be profiles across a coastal platform: Theory and example from the English Channel

V. Regard[1*], T. Dewez[2], D.L. Bourlès[3], R. S. Anderson[4], A. Duperret[5], S. Costa[6,] L. Leanni[3], E. Lasseur[2], K. Pedoja[7] and G. M. Maillet[8]

1. Université de Toulouse; UPS (OMP); CNRS; IRD; GET; 14 Av. Edouard Belin, F-31400 Toulouse, France.

2. BRGM; Risques Naturels; F-45060 Orléans, France

3. Aix Marseille Univ., CEREGE, UMR CNRS 6635, BP 80, 13545 Aix en Provence, France

4. University of Colorado at Boulder, Department of Geological Sciences and Institute of Arctic & Alpine Research – INSTAAR, UCB 450 Boulder CO 80309, USA

5. UMR 6294 LOMC CNRS – Université du Havre, Laboratoire Ondes et Milieux Complexes, 53 rue de Prony, BP540, 76058 Le Havre, France

6. Université Caen Basse Normandie, Geophen, CNRS, LETG, UMR 6554, F-14032 Caen, France

7. UMR CNRS 6143 Morphodynamique Continentale et Côtière (M2C), Université Caen Basse Normandie, 2-4 rue des Tilleuls, 14000 Caen, France

8. Faculté des Sciences, Université d'Angers, 02 Bd Lavoisier, 49045 Angers cedex 01, France

* corresponding author. e-mail: vincent.regard@get.obs-mip.fr; ph: +33 561332645; Fax: +33 561332560

Abstract

We explore a new method for documenting the long term retreat rate of sea cliffs based on measurements and modeling of ^{10}Be concentration transects across present-day shore platforms. The proposed forward numerical model relies on a scenario of sea level rise since the last deglaciation, and predicts the shape of ^{10}Be concentration transects as a function of prescribed cliff recession and vertical coastal platform downwearing rates. Two independent transect features allow fitting the long-term recession rate model to field observations: a sharp ^{10}Be concentration drop predicted at the former stationary location of the cliff during the last glacial period ~100 ka ago, and a characteristic dome shape whose magnitude is directly related to the recession rate of the cliff. A retreating chalk cliff site from the English Channel coast of France, at Mesnil Val, where the 7 m tidal range broadly exposes the shore platform, was selected to test the proposed method. Although retreat rates were too high to pinpoint the predicted ^{10}Be concentration drop at the last glacial cliff position, the ^{10}Be-concentration of the flints sampled across the shore platform are consistent with the expected dome shape. When modeled using the proper tidal range and proposed Holocene sea level rise history, the ^{10}Be data yield a cliff retreat rate since the mid-Holocene of 11-13 cm/yr. This is consistent with a 30-year-long measurement record, strongly supporting the utility of the ^{10}Be method.

Key-words

Seacliff; Cliff retreat; Shore platform; Beryllium-10; Holocene; Sea-level; Downwearing

1 Introduction

Emery and Kuhn (1982) estimated that 75% of the world's shoreline is rocky. Rocky sea-cliff collapse is therefore a major hazard in coastal environments. Evaluating this hazard requires better knowledge of cliff retreat rates. Given the episodic nature of cliff collapse events, such rates must be integrated over long enough time-spans to average over the full spectrum of events. To date, mapping the location of a receding cliff and deducing its recession rate has been accomplished largely through comparison of mapped cliff positions from aerial photographs or topographic maps (e.g., Costa et al., 2004; Dornbusch et al., 2006; Moore and Griggs, 2002). The corresponding time-span may reach two centuries in the very best cases, but is more typically of the order of 80 years. In general, as older maps and photos contain geometric inaccuracies and lower spatial resolution, the older the data source, and thus the longer the time-span, the less accurate the cliff retreat rate. Also, when trying to understand natural coastal systems, one would ideally avoid the period affected by human impacts on the system (e.g., Dornbusch et al., 2007); unfortunately, this coincides with when historical data become reliable. Measuring long-term "natural" retreat rate has therefore remained an elusive goal because of lack of information on cliff positions in the past.

Cosmogenic nuclides, and among them ^{10}Be resulting from spallation reactions on Si and O and thus accumulating in silica-rich rocks, hold the potential to meet this challenge. Cosmogenic nuclides produced within rocks down to a few meters below the surface (*in situ*-produced cosmogenic nuclides) record when rocks have been exposed to cosmic rays at a given location, even when the uppermost surface rocks are removed (for example, see Gosse and Phillips (2001) for a cosmogenic nuclide primer). The production rate of cosmogenic radionuclides at depth z is given by:

eq. 1 $$P = P_0 \exp(-z/z^*)$$

where the decay length scale z^* depends upon material density, ρ (either rock or water, the respective decay length scales being z_r^* and z_w^*): $z^* = \Lambda/\rho$; P_0 is the production rate at surface, which is dependent on the latitude and elevation of the sampling site, and Λ is an attenuation factor that depends upon the production reaction. According to their respective attenuation factors, the production due to spallation by neutrons, the most efficient of the processes, decays by an order of magnitude every ~2-3 meters (~5 m under water) while the production due to the less efficient muons extends over tens of meters (Braucher et al., 2003; Kim and Englert, 2004). For a given parcel of rock, the cosmogenic nuclide concentration N evolves according to the differential equation in which production and decay are incorporated:

eq. 2 $$dN/dt = P - \lambda N$$

λ being the decay constant. Cosmogenic nuclides have recently been used to quantify slowly eroding cliffs (<<10 cm/yr; Recorbet et al., 2010; Le Roux et al., 2009), but until now have not been employed to quantify recession rates of rapidly eroding coastal cliffs.

In this paper we propose a simple model for the concentrations of cosmogenic nuclides to be expected in rocks sampled across present-day shore platforms, and compare its predictions against measured concentrations to derive long-term cliff retreat rates. The model allows two ways of evaluating long-term recession rates: i) by locating where the cliff stood inactive during the last glacial period; ii) by analyzing the shape of cosmogenic nuclide concentration transects along the Holocene platform. We test our model at Mesnil-Val, a chalk cliff site along the French coast of the English Channel ("*La Manche*" in French).

1.1 Brief overview of processes driving coastal erosion

On rocky coasts, and particularly on chalky coasts, cliffs may retreat as fast as 20 cm/yr, while the shore platform undergoes downwearing (e.g., Stephenson and Kirk, 2000a; Stephenson and Kirk, 2000b; Trenhaile and Byrne, 1986). The processes responsible include: chemical weathering during tide water level fluctuations (Duperret et al., 2005; Kanyaya and Trenhaile, 2005; Stephenson and Kirk, 2000a; Sunamura, 1992), biological action (e.g., Nesteroff and Mélières, 1967), and the mechanical action of waves (e.g., de Lange and Moon, 2005; Stephenson and Kirk, 2000b). On chalky coasts along the English Channel, these processes result in a roughly linear coastline in plan-view, and a very shallowly sloping shore platform (typically ~1:150). This suggests that the overall effect of

erosion along the coast is relatively uniform in the long term and leads us to assume that cliff erosion is in fact also steady in the long term (100-1000 yr), averaging the short term stochastic behavior associated with 0.1-100 yr recurrence of sudden collapse events (Duperret et al., 2004; Hutchinson, 2002; Mortimore et al., 2004).

The model we develop is applied to a study site located on the southern English Channel shore, at Mesnil-Val (50°03'N, 1°20'E, Figure 1), where the cliff rises from 20 m up to 80 m, and the platform width ranges from 300 to 600 m. The average tidal range is ~7 m. Cliff lithology is Upper Cretaceous (Turonian to Coniacian) chalk, known as the Lewes Nodular Chalk Formation (Mortimore et al., 2004). Strength varies little, resulting in a planar platform with the exception of steps that are up to 40-cm high, corresponding to alternation of hardgrounds and softgrounds (Lasseur et al., 2009) (cf. Figure 1). The cliff at Mesnil Val has retreated at an average rate of ~15 cm/yr for the 1966-1995 period (Costa et al., 2004), but single collapse events can remove pieces as thick as 18 m (laser scanning observations processed by T. Dewez) that therefore correspond to roughly 120 years worth of erosion.

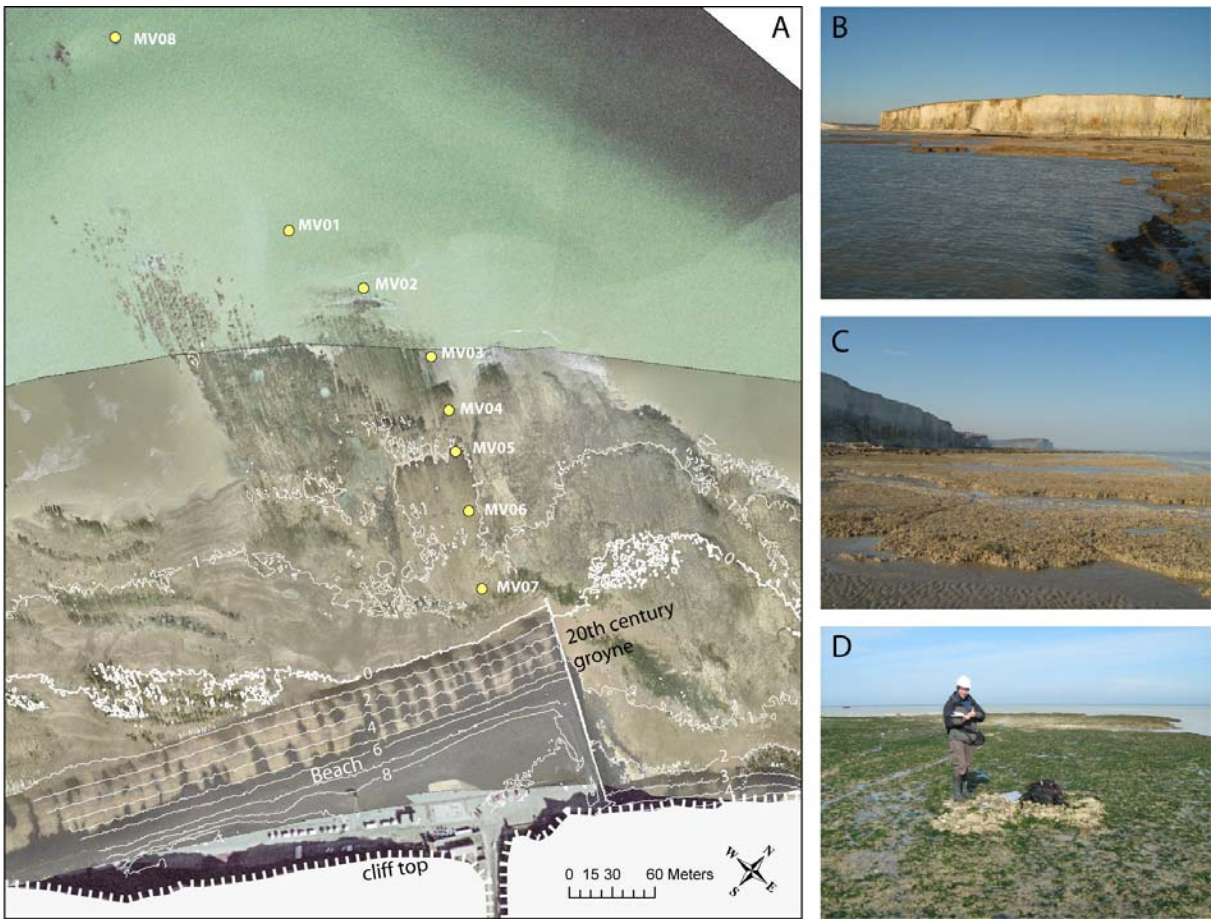

Figure 1. A. Aerial photograph of Mesnil Val site. Sample locations are shown; contour levels are drawn each meter (aerial LIDAR data), the 0 level (NGF reference) in bold (average water level is +0.43m NGF). Note the groyne dating back to the 20th century has had no long term effect on platform downwearing, but is clearly the cause of beach accumulation to the southwest. The photograph is not taken at very low tide, explaining the fact that all sampling sites are submerged. The cliff height is ~20 m, reaching 50-80 m less than 1 km away either northeast or southwest. B. to D. Site photos. Photo D. is the MV04 sampling site.

2 Simple model for cosmogenic nuclide concentration

2.1 Background

With the exception of coasts situated at relatively high latitude, almost every coast on Earth was left far inland during the last glacial maximum (LGM). If distant enough from LGM ice caps, they then experienced a rapid sea level rise from ~ -120 m 18 ka ago to roughly modern levels by ~6 ka BP (Clark et al., 1978). This is the case for the English Channel (Edwards, 2001; Edwards, 2006; Edwards and Horton, 2000; Lambeck, 1997; Lambeck et al., 1990; Peltier et al., 2002). Assuming that the cliff already existed during the former interglacial period, at an elevation within 5 m of current sea level (Siddall et al., 2006), sea-cliff evolution likely occurred in three stages (Figure 2).

Stage 1- During the last glaciation, sea level dropped by roughly 120 m, abandoning the cliff inland and left the platform to evolve subaerially for about 100 ka. Platform rocks thus accumulated cosmogenic nuclides down to several meters below the ground surface. Even if the last interglacial sea-level maximum was ~5 m above the current one (Siddall et al., 2006), the height difference being smaller than common platform relief (~10 m), the last interglacial platform was most likely exposed at an elevation comparable to the modern one.

Stage 2- When deglaciation started ~18 ka ago, sea level rose rapidly until it reached a plateau within ~5 m of present-day sea level (Edwards, 2001; Edwards, 2006; Lambeck, 1997; Peltier et al., 2002; Waller and Long, 2003) roughly 6 ka ago. By this time the sea had therefore reoccupied the abandoned platform and reinitiated cliff recession. Rocks previously shielded from cosmic rays by the cliff mass then became exposed to them and started to accumulate cosmogenic nuclides.

Stage 3- Today, the cliff is actively retreating while the shore platform is eroding vertically (lowering). To first order, the ratio of vertical erosion to lateral cliff retreat sets the slope of the shelf, here roughly 1: 150. Vertical downwearing does remove surface material, however, at a rate that is slow enough that cosmogenic nuclide concentrations accumulated at depth remain detectable. This is verified in the following calculations as well as in measured concentrations.

A principal goal of the paper is to model the dependence of the spatial pattern of concentration of ^{10}Be across the platform surface on cliff retreat rates using this simple exposure scenario.

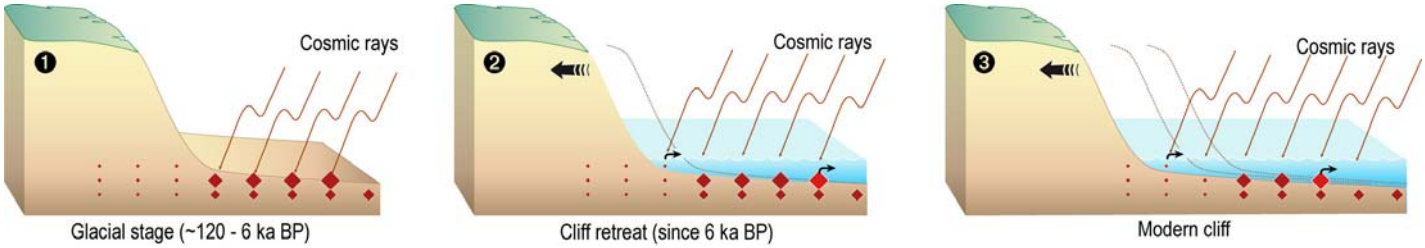

Figure 2. Stages of cliff evolution after the penultimate glacial period (see text for details). 1- During the last glacial period, the sea-cliff is abandoned on land and fossilized (it no longer moves). 2- The sea rises to a level close to the modern level (at 0±5m, ~6 ka BP). The cliff is retreating while the platform is downwearing (symbolized by the small black arrows). 3- Current setting. Diamond sizes are proportional to expected cosmogenic nuclide concentrations. Note that the former cliff position is marked by nothing but cosmogenic nuclide concentrations at, and below, platform surface.

2.2 Enrichment model, part 1: basic model without tides

The ^{10}Be concentration measured in a given sample is controlled by i) the *duration* of its exposure to cosmic rays, ii) its *depth* of exposure, and iii) additional *shielding* imposed by overlying bodies of material absorbing cosmic rays. In our ^{10}Be enrichment model, we assume that i) the platform in front of the glacial cliff was exposed to cosmic rays during roughly 100,000 years; ii) sea level rose to the present coastal platform about 6,000 yrs ago; iii) from then on, the cliff retreated at a constant rate; and iv) the shore platform vertical downwearing is proportional to horizontal cliff retreat (i.e., there is

conservation of the platform slope through time), the proportionality being set by the tangent of the platform slope α:

eq. 3 $w = v \tan \alpha$

where w is the downwearing rate and v is horizontal cliff retreat rate (Dornbusch and Robinson, 2011). The basic model takes water shielding into account, but for simplicity ignores factors like glacial-age cliff smoothing and diffusion, chalk weathering and vegetation shielding (see expected effects of these factors in the discussion section). The sharp step in concentration predicted in the following discussion represents an end-member case, and will likely be more diffuse in reality. The production P thus depends on the water depth z_w and the sample depth below the surface, the total shielding depth being: z_r+z_w. The instantaneous production rate (Equation 1) thus becomes:

eq. 4 $$P = P_0 \exp\left(-\left[z_r / z_r^* + z_w / z_w^* \right] \right)$$

Once the cliff has retreated over a site at a rate v, rock is eroded at a downwearing rate w (eq. 3), $z_r = z_s - wt$, where z_s is the depth below the cliff base (usually, the sea level) and t the time since the cliff retreated past this site. Similarly, $z_w = wt$.

As the characteristic time of the evolution of the system (a few thousand years) is much smaller than the roughly 1.4 Ma ^{10}Be half-life (Korschinek et al. (2010), Chmeleff et al. (2010)), we may safely ignore radioactive decay and the differential equation for the evolution of nuclide concentration becomes simply:

eq. 5 $$\frac{dN}{dt} = P = P_0 \exp\left(-\left[\frac{z_s - wt}{z_r^*} + \frac{wt}{z_w^*} \right] \right) = P_0 \exp\left(\frac{-z_s}{z_r^*} \right) \exp\left(wt \left[\frac{1}{z_r^*} - \frac{1}{z_w^*} \right] \right)$$

Eq. 5 leads to a timescale t^* defined by:

eq. 6 $$1/t^* = w/z_r^* - w/z_w^* = \frac{w(\rho_r - \rho_w)}{\Lambda} \quad \text{or} \quad t^* = \frac{\Lambda}{v \tan\alpha (\rho_r - \rho_w)}$$

To determine x, the distance to the cliff, we substitute $z_s = x \tan \alpha$ to obtain

eq. 7 $$N = \int_0^T P_0 \exp\left(-x \tan\alpha / z_r^* \right) \exp\left(t / t^* \right) dt = P_0 \exp\left(-x \tan\alpha / z_r^* \right) t^* \left(\exp\left(T / t^* \right) - 1 \right)$$

where T is the time since the cliff retreated over the sample site ($T = x/v = x \tan \alpha /w$). Thus:

eq. 8 $$N = P_0 \exp\left(\frac{-x \tan\alpha}{z_r^*} \right) \cdot t^* \cdot \left(\exp\left(\frac{x \tan\alpha}{w t^*} \right) - 1 \right)$$

In the latter expression a natural length scale $\beta = w\, t^*/\tan \alpha$ appears. Consequently,

eq. 9 $$N = P_0 \exp\left(-x \tan\alpha / z_r^* \right) \frac{\beta}{v} \left(\exp\left(x/\beta \right) - 1 \right) \quad \text{and} \quad \beta = \Lambda / \left((\rho_r - \rho_w) \tan\alpha \right)$$

The predicted ^{10}Be concentrations at the study site are computed using a surface production rate by spallation estimated from the CRONUS Web calculator 2.2.1 (Balco et al., 2008) of 4.34 at/g/yr. Water density is taken to be 1,050 kg.m^{-3} to acknowledge suspended sediment, and the chalk bulk density is assumed to be 1,800 kg.m^{-3} (Mortimore et al., 2004). The model was run for a wide (1200 m wide) platform with a slope (1:240) representative of Mesnil Val sampling site (Figure 3) (Note that this is a little less steep than elsewhere along the Normandy Coast). Two models are presented: the analytic model that takes into account only production by spallation (eq. 8 and eq. 9); and the numerical model that takes into account all production reactions (neutrons, fast muons and negative muons). The latter is then implemented for tides. Production rates for slow and fast muons are, respectively, 0.012 and 0.039 at/g/yr at the surface (Braucher et al. 2011). The attenuation lengths Λ are taken to be 1,600 kg.m^{-2} for neutrons, 15,000 kg.m^{-2} for negative muons and 43,200 kg.m^{-2} for

fast muons (Heisinger et al. 2002a; 2002b). In accord with recent measurements, the ^{10}Be half-life is taken to be 1.39 ± 0.01 Ma (Chmeleff et al., 2010; Korschinek et al., 2010).

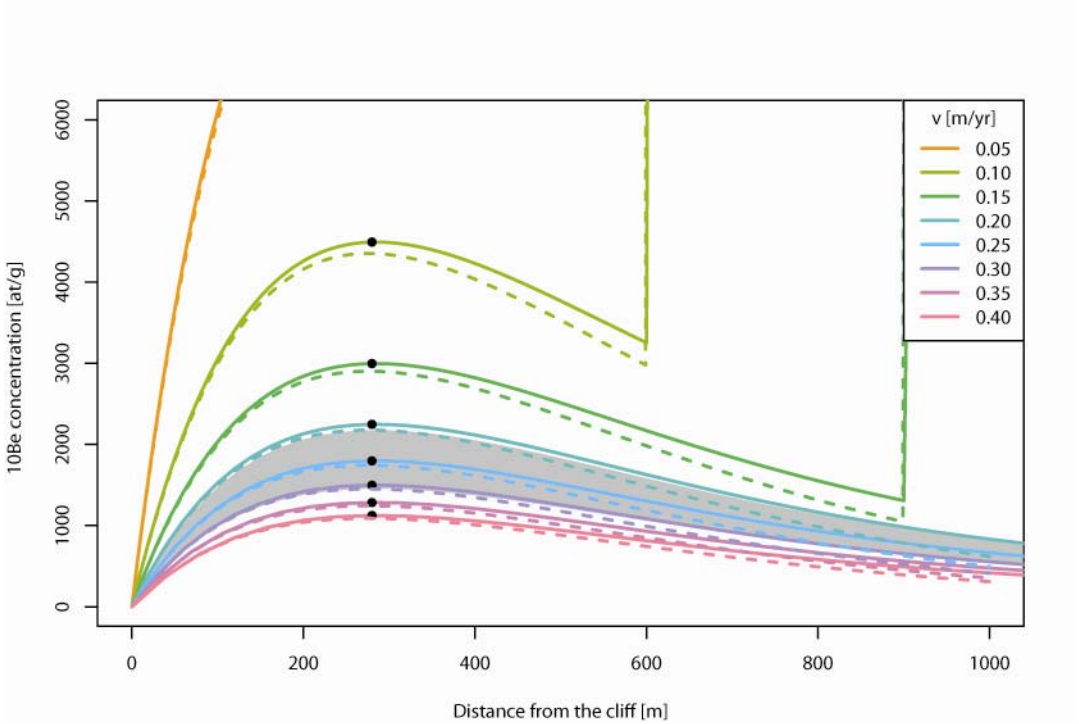

Figure 3. Predicted 10Be concentration on rocks on the platform with no tidal effect. The color of the curve indicate the cliff retreat rate. Dashed lines are calculated for a model with only neutron production. The continuous lines represent models with the different production sources. The former cliff position corresponding to a scenario with a sea level at its position since 6 ka and a retreat velocity of 10 cm/yr is represented. Peak locations are shown by black dots. Grey pattern represents the 20% confidence area around the v=0.25 m/yr case; it represents the typical uncertainty around the data points (cf. Table 1).

Two features are of interest in the results. First, the model predicts ten times more ^{10}Be in the old glacial platform than on the new Holocene-cut platform, with a sharp concentration step in between. Second, ^{10}Be concentration profiles across the Holocene platform are expected to display an arch that is small in amplitude but, providing top class AMS facilities are employed, should remain detectable for retreat rates up to 30 cm/yr. At present, analytical resolution is sufficiently precise to discriminate between rates of 20, 25 and 30 cm/yr (Figure 3). To make use of this model with real data, pinpointing the glacial to Holocene concentration step is by far the most robust method for deducing long term (~6 ka) recession rates. Failing that, modeled concentration transects show a bump discriminative of different cliff retreat rates. This bump results from the competition between vertical downwearing and oceanward increases in sea water-shielding and duration of exposure to cosmic rays. The location of the maximum in ^{10}Be concentration (x_p) does not depend on cliff retreat rate: it should occur at $x_p=\beta \ln(\rho_r/\rho_w)$ ($dN/dx=0$ in eq. 9). At our study site this is 276 m. However, the peak concentration N_{max} depends inversely on the cliff retreat rate: the faster the retreat rate, the lower the peak concentration.

eq. 10 $$N_{max} = 1/v \cdot P_0 \frac{\Lambda}{\rho_w \cdot \tan(\alpha)} \cdot \exp\left(\frac{\rho_r}{\rho_r - \rho_w} \ln(\rho_r/\rho_w)\right)$$

2.3 Enrichment model, part 2: with tides

Production in the presence of tides, which plays the role of a cyclic shield, requires that we integrate the production rate over a tidal cycle. The instantaneous production is

eq. 11 $$P(t) = P_0 \exp\left(-H/z_w^*\right)$$

where H is the instantaneous water level. Taking z_w to represent the mean sea level, with tides of amplitude ΔH and period T, the production history over a tidal cycle becomes

eq. 12 $$P(t) = P_0 \exp\left(-\frac{z_w + \Delta H \sin(2\pi t / T)}{z_w^*}\right)$$

This may be simplified to

eq. 13 $$P(t) = \left[P_0 \exp\left(-\frac{z_w}{z_w^*}\right)\right] \exp\left(-\frac{\Delta H \sin(2\pi t / T)}{z_w^*}\right)$$

in which the first term in brackets captures the effect of mean water depth, and the second term represents the effect of the tidal cycle. Note that the sign of the argument in the 2nd term switches between high tides (sin>0) and low tides (sin<0).

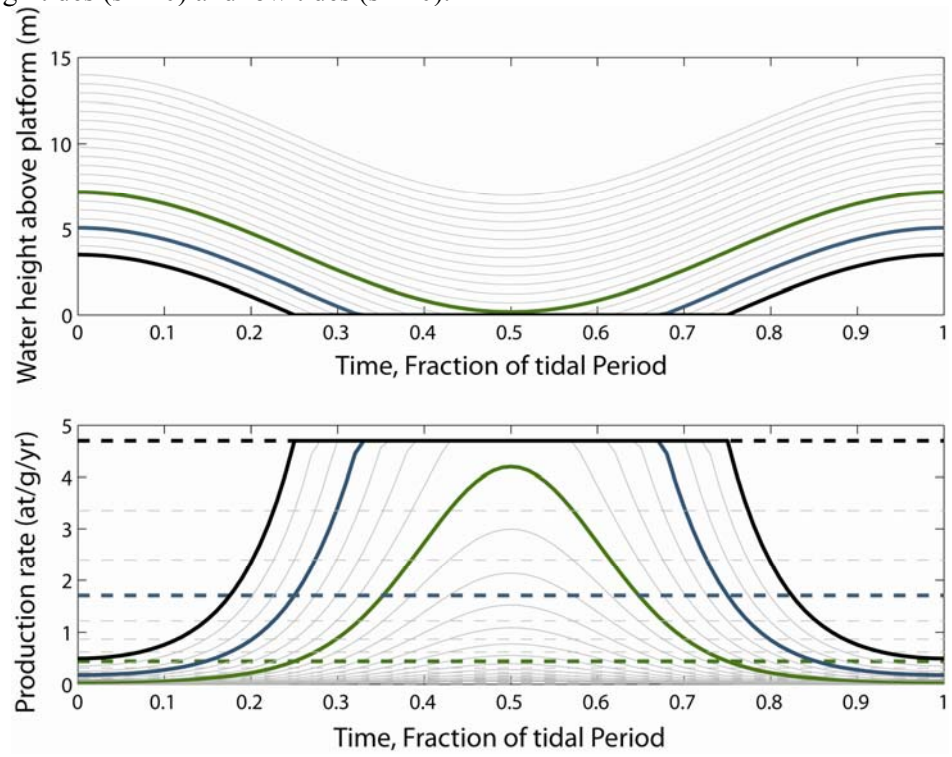

*Figure 4. Production over the tidal cycle, for various sites along a platform that slopes at 1/150. Tidal cycle with amplitude of 3.5m, full range of tides = 7m. Top: water level history over the tidal cycle. For locations > 3.5m*150 (bold green case), the full tidal cycle is experienced, whereas at all shallower depths the cycle is truncated as the platform is fully exposed. Bottom: production history over the tidal cycle. Solid lines: case with tides. Dashed lines: case with no tides, for comparison. For very shallow depths (e.g. bold black lines), production is damped by tides swamping the platform, leading to a reduction in production relative to the no tide case. At greater depths (e.g. bold blue case and beyond), the enhanced production during low tide overwhelms the damped production during high tides, leading to greater total production over the tidal cycle.*

We illustrate the numerical simulation of production rate as a function of tidal amplitude in Figure 4. The essence of the tidal effect is to damp the expected tidal cycle average production rate in shallow water, and to enhance it in deeper water. As depicted in Figure 5, in shallow water the tide rises above the platform, thereby reducing the production during high tides, while at low tides the platform is exposed and receives the full production rate (the plateau on all production rate histories). The total concentration accumulated during the tidal cycle is therefore lower than would accumulate if there were no tide (area under the curve is smaller than the area under the dashed line, Figure 4). In deeper water, the expected production rate in the absence of tides declines exponentially (Figure 5, dashed lines). Eventually the water is deep enough for the enhanced production during low tide to

outweigh the damped production during high tide; for depths greater than this, production during the tidal cycle exceeds that expected in the absence of tides. For parts of the platform with depths greater than the tidal amplitude, the production exceeds the no-tide case by a fixed ratio, *R* (Figure 5). We can see this by examination of the integrated form of equation 13:

eq. 14
$$R = \frac{P_0 \cdot e^{-z_w / z_w^*} \int_0^T e^{-\Delta H \sin(2\pi t / T)/ z_w^*} dt}{P_0 \cdot T e^{-z_w / z_w^*}} = \frac{1}{T} \int_0^T e^{-\Delta H \sin(2\pi t / T)/ z_w^*} dt$$

In other words, the ratio of production in the presence of tides to that in the absence of tides is the integral of the exponential function with a sinusoidal argument. This integral is a function of $\Delta H/z^*_w$. Note that when ΔH=0 (no tide case), the integral becomes T and the ratio is 1, as expected. The ratio increases non-linearly with tidal amplitude due to the asymmetry of the exponential function: times of negative values are reduced and bounded between 0 and 1, while times of positive values are enhanced and are bounded between 1 and infinity. While there is no closed form solution for this definite integral, the leading two terms in the expansion of *exp(cos(x))* result in $R = 1 + \frac{1}{4}(\Delta H/z^*_w)^2$. The effect therefore goes roughly as the square of the tidal amplitude.

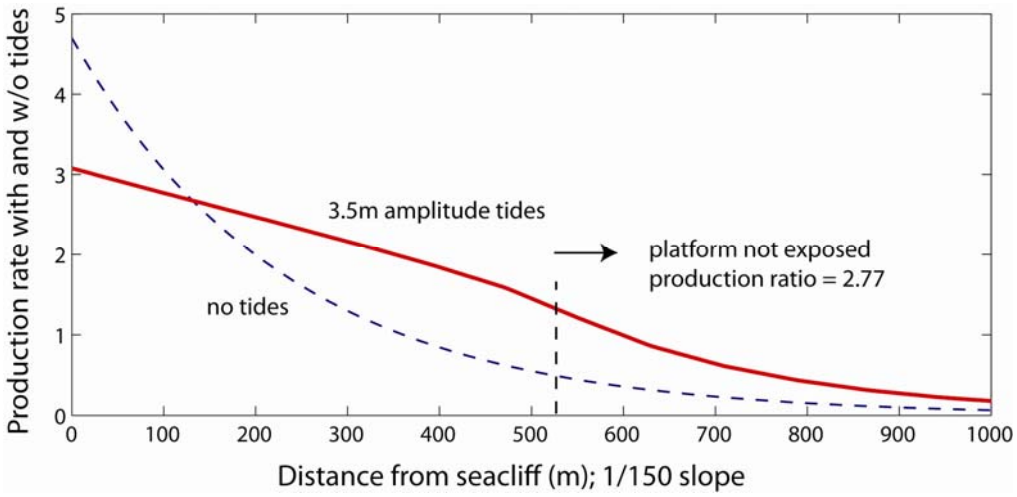

Figure 5. Difference of production over a tidal cycle between a case without tides and a case with 3.5 m amplitude tides (tidal range = 7 m) and 1/150 platform slope. The ratio between the tide and no-tide cases increases with the distance from the cliff. In locations beyond which the platform is never exposed at low tide, the ratio becomes a constant, at R=2.77 (see text).

The fluctuation in tidal amplitude through the lunar cycle (i.e., from neap to spring tide) is not taken into account here. The tidal effect on ^{10}Be concentration over the platform is shown on Figure 6. Note that the bump in ^{10}Be concentration becomes smoother as the tidal range increases, illustrating the asymmetry effect. Thus, the higher the tidal range, the smaller the amplitude of the bump in concentration and hence the more difficult it will be to locate and to measure.

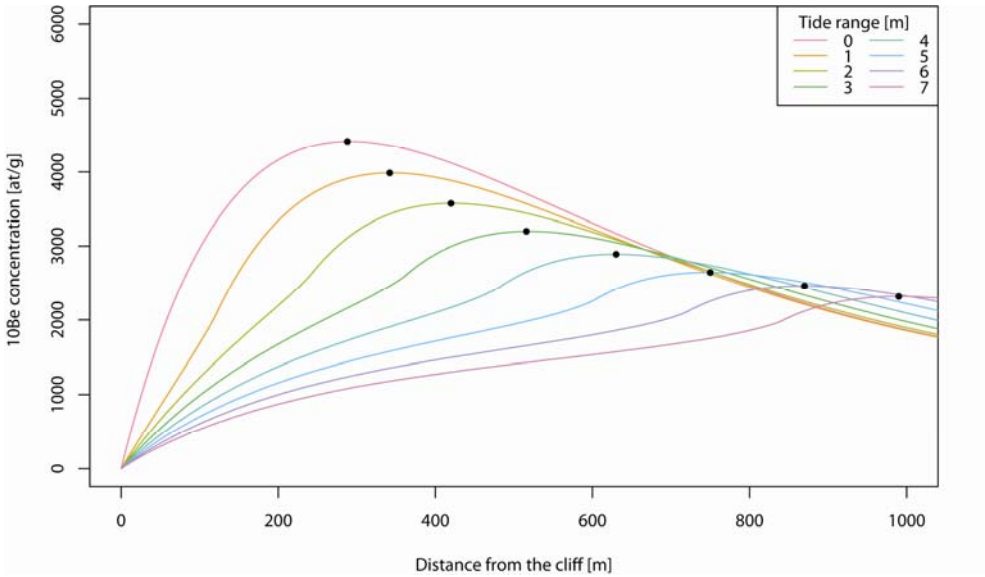

Figure 6. Predicted 10Be concentration on rocks on the platform depending on the tide range. Cliff retreat rate is 0.1 m/yr, peak locations are shown by black dots. Note that the curves are drawn up to 1000 m while if sea returned to its current level at 6 ky BP, they should show a step at 600 m.

2.4 Enrichment model part 3: a rising sea level

Fitting the ^{10}Be data (see next section) required taking into account the Holocene sea level rise. Sea level rose by several meters during the Holocene recession history of the cliff. The retreat rate of the seacliff, v, and the rate of sea level rise, dS/dt, combine to govern the trajectory of the inner edge of the cliff (Figure 7). That this trajectory is upward means that to explain the present geometry (angle) of the shore platform requires less vertical erosion than would be required in the absence of sea level rise. This alters the degree to which the ^{10}Be profile is truncated, and should lead to higher ^{10}Be concentrations.

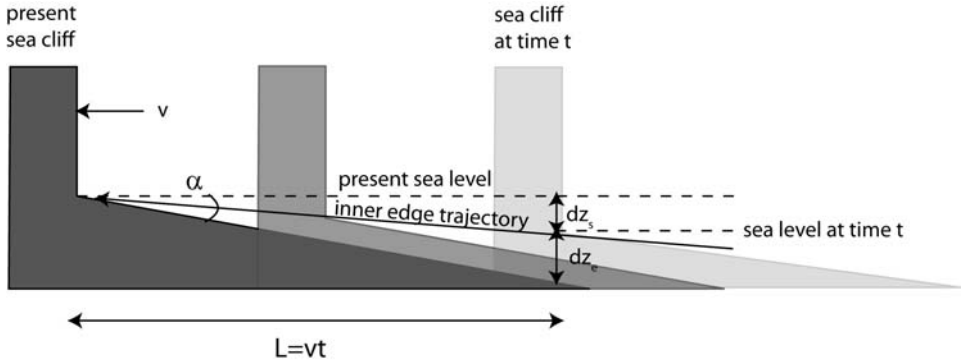

Figure 7. Sketch of platform geometry evolution during erosion when sea level rises. See text for further explanation.

We sketch the situation in Figure 7. The slope of the present platform depends on the rate of rise of the inner edge of the seacliff, the rate of sea level rise, and the downwearing rate of the platform, w. For a location on the platform at a distance L from the present cliff, the cliff retreated over that site a time t ago, such that $L=vt$. Since that time the sea level has risen by $dz_s = t\, dS/dt$, while vertical erosion of the platform at a rate w has lowered the platform by $dz_e = wt$. The sum of these sets the mean water depth at that site at $z_w = dz_e + dz_s$. For small slopes,

eq. 15 $$\alpha = \tan\alpha = {z_w}/{L} = \frac{dz_s + dz_e}{L} = \frac{(dS/dt)t + wt}{vt}$$

Rearranging, if the measured present day slope of the shore platform is α, then the required vertical erosion rate becomes

eq. 16 $$w = v\alpha - \frac{dS}{dt}$$

Because this will result in longer residence times in the production zone (or, equivalently, less loss of the inventory due to erosion), the ^{10}Be concentrations in the presence of rising sea level will be higher than those in a steady sea level scenario.

3 A natural test: ^{10}Be on Normandy shore platform

3.1 Sampling and processing

In order to test the validity of our theoretical model described above, *in-situ* outcropping flint samples were extracted from the chalk platform along an across-shore transect, attempting to reach the furthest distance possible from the cliff (up to 600 m from the cliff, a fair weather day of strong equinox tide, cf. Figure 1). There is one exception to this sampling scheme, as finding *in-situ* flint was challenging. Sample MV-08 was extracted from the side of a block 80 centimeters below its top surface. This means that ^{10}Be concentration is lower than if it had been sampled from the surface: in the following calculations, the equivalent surface concentration is computed, assuming a rock density of 1800 g/cm^3 (cf. Table 1).

Table 1. Sample 10Be concentrations

Sample ID	Depth (cm)	Size (cm)	Number of clasts	Distance from cliff* (m)	±	Mass of pure flint dissolved (g)	Measured Be10/Be9	Uncertainty Be10/Be9 (%)	10Be concentration (at/g)	±	± (%)	10Be surface conc.† (at/g)	±
MV-08	80	5	2	609	5	29.18	6.6921E-15	10.49	1504	642	42.69	2562	1341
MV-01	0	20	1	460	5	29.92	1.1257E-14	6.50	4568	640	14.01		
MV-02	0	5	1	423	5	24.78	9.7594E-15	8.03	4270	803	18.81		
MV-03	0	7	1	358	5	30.93	9.0181E-15	9.10	2950	667	22.61		
MV-04	0	10	1	320	5	31.73	9.1295E-15	8.28	2948	617	20.93		
MV-05	0	7	2	290	5	30.79	8.7347E-15	7.79	2768	595	21.50		
MV-06	0	10	1	249	5	29.91	9.7071E-15	6.86	3503	604	17.24		
MV-07	0	10	1	188	5	30.82	9.4628E-15	11.95	3255	844	25.93		
blank							4.5434E-15	13.00					

* measured with a laser distance meter

†corrected for partial shielding by chalk instead of water. MV-08 was collected on the side of a block at 80 cm below its surface. We considered it was half shielded by 80 cm of overlying chalk, half by overlying 80 cm of rock, water or air, with the same probability.

Samples were prepared for Accelerator Mass Spectrometry (AMS) ^{10}Be measurements following chemical procedures adapted from Brown et al. (1991) and Merchel and Herpers (1999). Samples were first crushed and sieved. Pure flint was obtained from the 250-500 µm fraction by repeated H_2SiF_6 - HCl etching; atmospheric ^{10}Be was subsequently eliminated by sequential dissolutions with diluted HF. Prior to complete HF digestion of silica, a weighted 100 µl of a 3025 ppm home-made ^{9}Be solution with known and very low ^{10}Be/^{9}Be ratio was added as a carrier for ^{10}Be. Because the thus added ^{9}Be concentration overwhelmed by at least 3 orders of magnitude the natural ^{9}Be concentration, it definitively fixed the ^{10}Be/^{9}Be ratio before any chemical manipulation and allows therefore calculating the sample ^{10}Be concentration from the ^{10}Be/^{9}Be ratio measured by AMS. The remaining solutions were dried, diluted in HCl, purified by anion and cation exchange columns, followed by Be extraction by alkaline precipitations. The final precipitate was dried, and heated at 900°C to obtain BeO. Beryllium oxide was mixed with 325 mesh niobium powder prior to measurement at ASTER, the French AMS national facility located at CEREGE, Aix en Provence. All ^{10}Be concentrations are normalized to ^{10}Be/^{9}Be SRM 4325 NIST reference material with an assigned value of $(2.79\pm0.03).10^{-11}$. This standardization is equivalent to 07KNSTD within rounding error. The ^{10}Be half-life of $(1.39 \pm 0.01) \times 10^6$ years used is that recently recommended by Korschinek et al. (2010) and Chmeleff et al. (2010), according to their two independent measurements. Analytical uncertainties (reported as 1σ) include a conservative 0.5% external uncertainty based on long-term measurements of standards, a one

sigma statistical error on counted ^{10}Be events, and the uncertainty associated with the chemical and analytical blank correction (the ^{10}Be/^{9}Be blank ratio was (4.54 ± 0.59) x 10^{-15}, cf. Table 1).

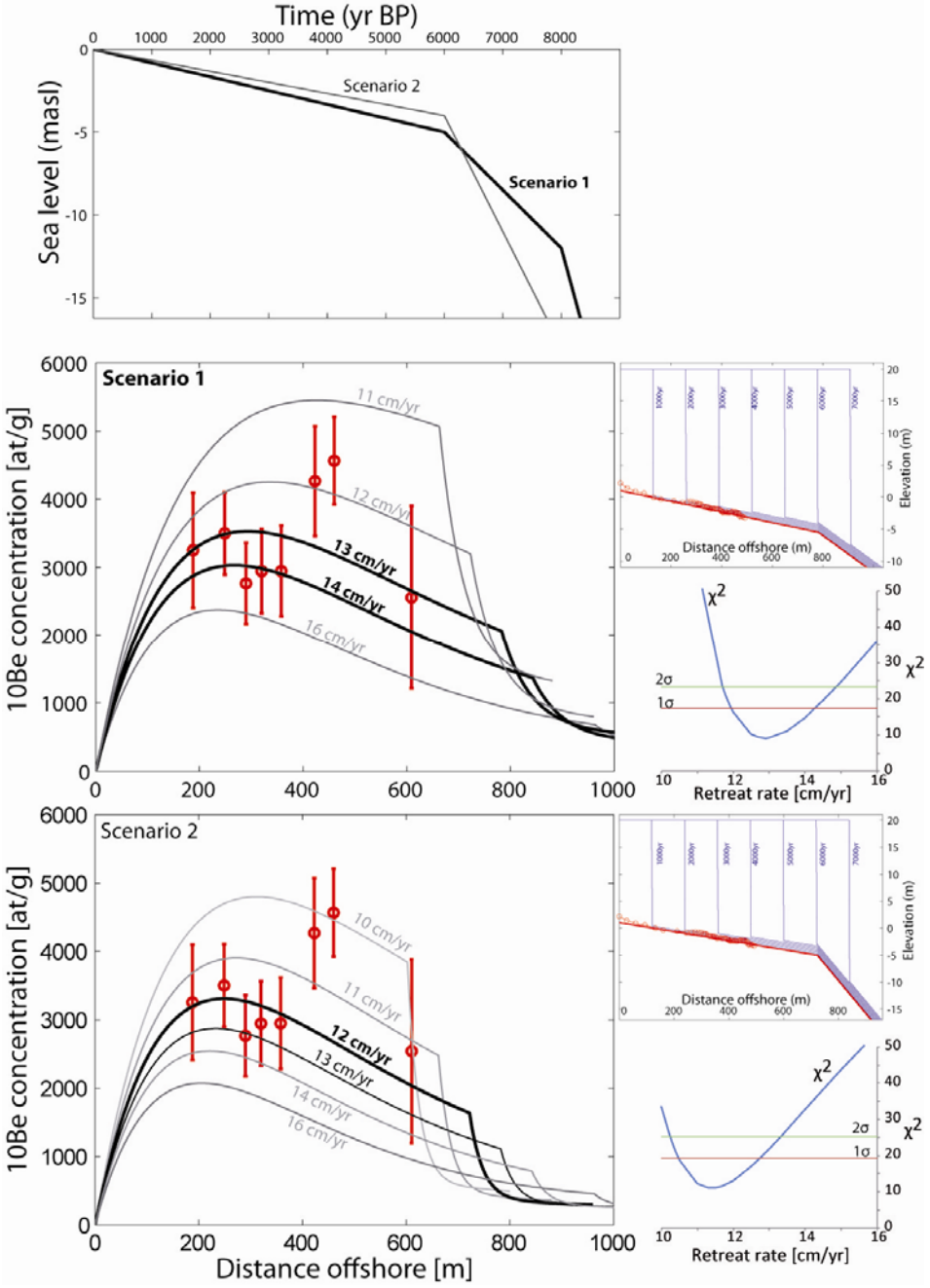

Figure 8. 10Be concentrations in platform samples vs. distance from the cliff, and models of 10Be profiles. A. 2 sea level rise scenarios from Massey et al. (2008) and Lambeck (1997), respectively. B. The predicted 10Be concentration curves are plotted for different long term cliff retreat rates according to sea level rise scenario 1. To the right, top inset displays the different topographic/bathymetric profiles (at 1000 yr intervals), and the fit to the platform GPS profile (circles). The platform lowering rate is chosen to assure that the fit of the final observed profile is optimized (see text, eqn. 16). Bottom inset show the χ2 metric of quality of fit. The best-fit value (χ2 minimum value) is 12.8 cm/yr (χ2=9.2). Corresponding 1σ (68%) and 2σ (95%) confidence intervals are, respectively, [11.9-14.3 cm/yr] and [11.7-14.9 cm/yr]. C. Same as B for scenario 2. Corresponding best fit, 1σ (68%) and 2σ (95%) confidence intervals are, respectively, 11.4 cm/yr (χ2=11.0), [10.5-12.7 cm/yr] and [10.2-13.3 cm/yr].

Due to the short exposure duration of the samples at low elevations (sea level), the accumulated in situ-produced cosmogenic nuclide concentrations are low and therefore so are the measured ^{10}Be/Be

ratios and the numbers of events detected by AMS. Consequently, combining the uncertainty due to the chemical and analytical blank correction with the statistical uncertainties on the low $^{10}Be/^{9}Be$ ratios leads to large uncertainties associated with the calculated exposure ages (up to 43%). These may only be reduced by processing a larger mass of material. However, even with such uncertainties, we argue that one may constrain the long-term retreat rate, with acceptable uncertainties.

3.2 Cliff retreat rates at Mesnil-Val

At Mesnil-Val, despite sampling as far as 600 m away from the cliff face, we did not find the expected signature of the glacial cliff position. This implies that cliff retreat rate integrated over 6000 yrs cannot be lower than 10 cm/yr (Figure 8). Further, we found it impossible to fit correctly the data without taking into account the Holocene sea level rise. Indeed, a best-fit can be obtained with v=10 cm/yr, which properly fails to fit the data well: the resulting χ^2 is high (χ^2>70). Using the latest published sea level history for the Devon coastline (on the other side of the English Channel; Massey et al. 2008), and assuming that the tidal range has not varied during the last 8 ka (Uehara et al. 2006), the data are best fit by a cliff retreat rate $v \approx 0.13^{+0.02}_{-0.01}$ m/yr (scenario 1, Figure 8). This evaluation depends on the sea-level history used: a slightly different sea level history (i.e., Lambeck 1997) leads to a slightly lower cliff retreat rate ($v \approx 0.114 \pm 0.01$ m/yr (scenario 2, Figure 8)). We note, however, the importance of the knowledge of the accurate sea level history on the ^{10}Be concentration evolution across the shore platform. Further, the sea level histories measured in nearby coastlines agree for the last 5 kyrs but diverge for sea level evolution prior to the mid-Holocene. This leads to more confidence in the 'recent' cliff retreat rate deduced from our ^{10}Be platform profile; our results are not sensitive to the earlier sea-level history. On the basis of Figure 8 and published sea level curves, the discrepancy between the sea level scenarios is small for the first ~400 m (last ~3000 yrs). We are therefore confident of the mean retreat rates calculated by the model over this interval.

4 Discussion: how to measure the long-term retreat rate?

The numerical and simplified exposure model results presented here highlight two features that can be employed to determine long-term cliff recession rates. First, one can trace back the location of the last glacial cliff position. Second, one can fit the spatial pattern of concentration on the platform to derive cliff recession rates.

4.1 First method: last glacial cliff position

This method relies on the position of the cliff that was exposed and stable during the last glacial cycle sea level lowstand. The calculations were made for a cliff remaining vertical during the glaciation, with neither soil development nor cliff diffusion, and an instantaneous return of the sea to its present level at a well-known date. In addition, cliff retreat is assumed to be constant, and platform slope is assumed to be uniform ($w=v \tan \alpha$, eq. 3). Exploration of the biases introduced by failure of these hypotheses shows that if they lead to a smoothing of the step, the biases do not alter its position (Figure 9). Finally, the principal source of uncertainty is the sea level history. This is site-specific due to spatial complexity of the glacio-isostatic adjustment field, but in general sea-level returned to a level close to the current one at ~5-6 ka BP, except in regions close to ice sheet margins (Clark et al., 1978). Local sea-level curves have already been produced by studies based on glacioisostasy (cf. Lambeck, 1997), sedimentation (e.g., Devillers et al., 2007; e.g., Edwards, 2006; Kiden et al., 2002), and fauna (e.g., Kayanne et al., 1993; Massey et al., 2008; Morhange et al., 2001; Smith et al., 2007). Such local studies will help to constrain the proper sea-level history.

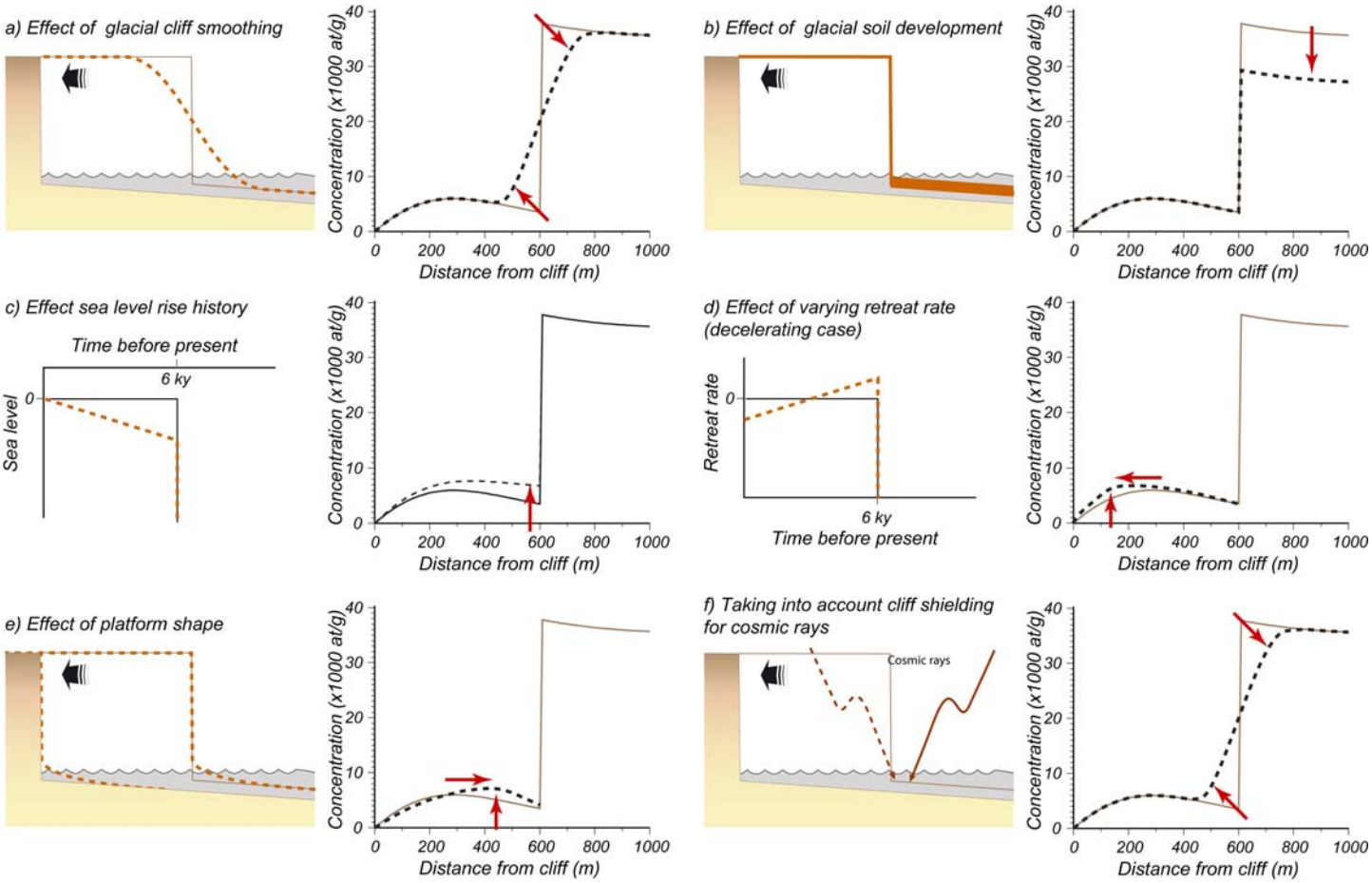

Figure 9. Qualitative variations in the 10Be concentration curve shape after taking into account the simplifications made in the main model. Note none of the factors we have illustrated changes the location of the concentration step. The main simplifications done are: (a, b) glacial surface processes are neglected. They encompass 2 main processes: cliff degradation and soil development. (a) Cliff degradation should change the profile by smoothing the concentration step. For a usual diffusion coefficient of □~10-3 m2/yr in 100 ky, the expected width of eroded material at cliff toe is ~half the cliff height (<< 50 m here, S. Carretier pers. comm.). (b) Soil development would affect up to one meter at platform surface, partially shielding deeper rocks; it would decrease the step magnitude, but not its location. (c) sea level history is very simple, with no sea acting on the platform before ~6 kyr and sea level at its modern value since then. A more complex history implies a smaller step. (d) the retreat rate is constant. A changing retreat rate would affect the concentration curve shapes, not the step location. (e) the platform lowering is considered proportional to the cliff retreat and the tangent of platform slope α. This is a classical assumption and is supported by an almost uniform slope of the platform (verified at Mesnil-Val). In addition we verify the section we use displays no step greater than ½ m (see site map), this process should not be significant with regard to the uncertainties on cosmogenic nuclide concentration data. (f) cliff shielding and lateral cosmic ray action are neglected. In practical, this must be important for the areas close to the cliff (the first 50 m); we base our reasoning on all the platform up to 600 m of a relatively low cliff (20-30 m at the place of the profile, to be compared to the maximal height of 80 m found at Mesnil-Val), hence this assumption must have small effects on the curves found.

This method depends on the technical ability to locate the step in concentration associated with the LGM cliff position, which could have been smoothed (Figure 9). Many samples are thus required for reliable location. Moreover, one can observe that the step decreases with cliff retreat rate, because the higher the cliff retreat rate, the higher the platform erosion/downwearing must be in order to maintain the observed low angle of the platform. Assuming that during the glacial period the concentration

acquired was N_h, an approximate value of the concentration step (S_N), considering only production by neutrons and no decay, is given by:

$$\text{eq. 17} \qquad S_N = H_h \cdot \exp\left(-v\frac{MIG}{\Lambda\rho_r}\cdot\tan\alpha\right)$$

where *MIG* is the time at which sea returns to its present level. Equation 17 implies that S_N decreases exponentially with *v*. At our study site, the predicted concentration step S_N is roughly 35,000 at/g for a cliff retreat rate (*v)* of *0.1 m/yr*, but quickly decreases to S_N*~2000 at/g* for *v=0.25 m/yr*; this latter value would not be discernible given present measurement methods. In addition, we note that the faster the cliff retreat rate is, the farther from the cliff the step will be located, rendering it harder to locate. For example, for *v=0.2 m/yr,* the step would be located ~1.2 km from the modern cliff, which is beyond the distance one can access on the shelf given even the high tidal range at our field site.

In summary, locating the step in ^{10}Be concentration may be easy if the cliff has not been smoothed too much during the glacial period, if cliff retreat has not been too rapid, and the platform slope not too steep. From our experience, platforms generally have gentle slopes and retreat rates are lower than *0.25m/yr*; thus, the two latter conditions will usually be met. The degree to which a seacliff will decay while subaerially exposed during glacial periods is less known, and likely highly dependent upon the cliff material properties.

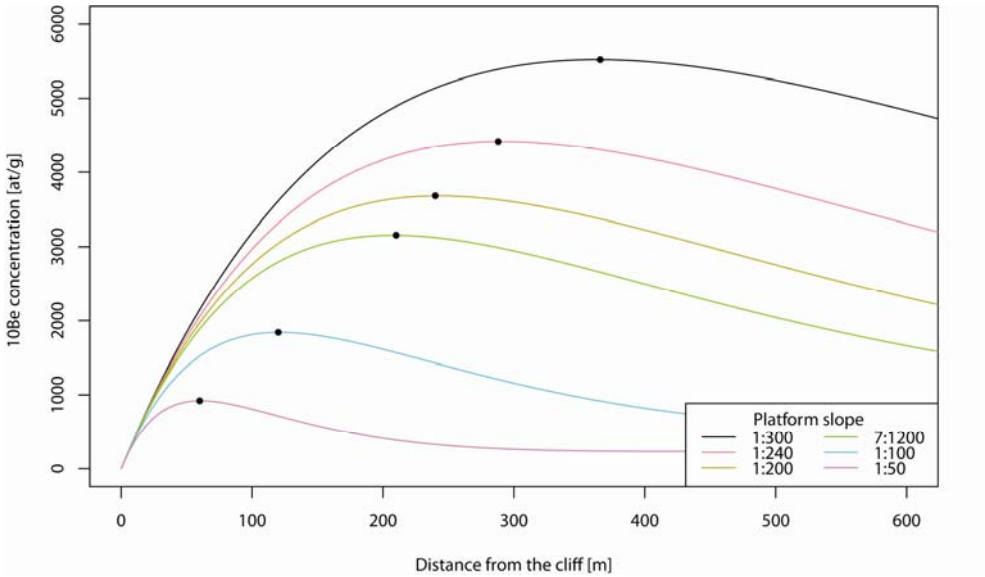

Figure 10. Predicted 10Be concentration on rocks on the platform depending on the platform slope. Cliff retreat rate is 0.1 m/yr, peak locations are shown by black dots.

4.2 Second method: bump location

The second method depends on the expected bump in ^{10}Be concentration across the platform. Without accounting for tides, its position must be found at $x_p=\beta \ln(\rho_r/\rho_w)$. In nature, most of the time $1.6<\rho_r/\rho_w<2.6$, leading to $0.5<\ln(\rho_r/\rho_w)<1$. Thus x_p depends mostly on $\beta = w\,t^*/\tan\alpha$ To ensure an ability to determine former cliff position, β must be smaller than the former cliff position. In turn, failure of this condition would allow the first method to be applied, except for high cliff retreat rates, since the peak concentration N_{max} decreases with the cliff retreat rates. Peak position also depends on the platform slope: the steeper the slope of the platform, the smaller the amplitude of the bump (Figure 10). We note that, in general, steep platforms are associated with lower cliff retreat rates (Sunamura, 1992).

Incorporation of tides leads to a more complicated trend. The bump migrates offshore and becomes less pronounced with increasing tidal range.

We note that bump amplitude and location are highly dependent on properties of a local setting (e.g., rock density). A bump of significant amplitude would preferentially be observed in settings with low tidal ranges, gentle slopes, and retreat rates probably ranging from ~2 to ~20 cm/yr.

Finally, refinement of the method to incorporate a more detailed Holocene sea level history is required, as this alters the history of downwearing rate and hence the pattern of concentration across the platform.

4.3 Long term retreat rates in Mesnil-Val

At Mesnil-Val, the absence of any step in ^{10}Be concentration as far as 600 m from the modern cliff toe implies a minimum Holocene averaged retreat rate greater than 10 cm/yr. Modeling of the arch in ^{10}Be concentration on the platform indicates a long-term cliff retreat rate of ~11-13 cm/yr (1σ confidence interval between 10.5 and 14.3 cm/yr), valid over ~3000 yrs. This is surprisingly consistent with modern observations of ~15 cm/yr (Costa et al., 2004). Our method therefore has strong potential for documentation of long-term coastal evolution that establishes the context for evaluation of anthropogenic effects.

In this scheme, the cliff retreat rate, platform slope and sea level history fix the platform downwearing rate. Our two scenarios predict average downwearing rates (eq. 16) of 0.42 and 0.17 mm/yr respectively (1.5 to 3 ‰ of the cliff retreat rate). As one can see from eq. 16 this is very sensitive to the assumed rate of recent sea-level rise (dS/dt). These downwearing rates are close to the lowest average downwearing rates measured by micro-erosion meters (MEMs) along chalk shores on both sides of the English Channel; we note that these field methods to date have low reproducibility (Foote et al. 2006). Future efforts may focus on a precise and long-term downwearing rate measurement to untangle these scenarios.

5 Conclusions

We propose a method to evaluate long-term cliff retreat rate based on the pattern of cosmogenic nuclide concentration across a shore platform. The method developed both analytically and numerically identifies the best conditions to reach a reliable result: the gently sloping site must have undergone moderate retreat rates (less than ~30 cm/yr). Under these conditions, the most reliable method is to locate the seacliff position during the last glacial, indicated by a discrete step in the ^{10}Be concentrations of platform samples. However, depending upon the setting, this location may now be drowned in water so deep that it is very difficult to sample. In this case, information can be obtained from cosmogenic nuclide concentration profiles across the platform that display a characteristic bump whose magnitude is a function of cliff retreat rate. Documentation of the detailed shape of such bumps could allow assessment of how steady the cliff retreat rate has been since Holocene sea level rise stabilized at roughly 6 ka, and whether the pattern is consistent with independently measured late Holocene sea level histories. A high tidal range and a shallow slope of the platform can combine to allow sampling of wide platforms that are most likely to contain such information about cliff retreat history. Application to the English Channel coast at Mesnil-Val, where tides have a 7 m range, and the platform is indeed very shallowly sloped, suggests long-term cliff retreat rate of 11-13 cm/yr that are remarkably consistent with modern observations of ~15 cm/yr. This success bodes well for application to other coastlines with similar attributes.

Acknowledgements

C. Cavare-Hester has drawn the sketch of Figure 2. This work benefited from a couple of years of observation by BRGM (internal project EVOLGEOM driven by TD). We thank the French SHOM/INSU RELIEFS program (“rocky coast erosion: from observation to modeling”, driven by VR) and BRGM (Bureau des Recherches Géologiques et Minières) for support. We thank D. Farber, S. Carretier, J. Martinod and D. Fink for encouraging remarks. We are indebted to A. Matmon and 3 anonymous reviewers for their constructive criticisms. The ^{10}Be measurements were performed at the ASTER AMS national facility (CEREGE, Aix en Provence) that is supported by the INSU/CNRS, the French Ministry of Research and Higher Education, IRD and CEA. We thank L. Léanni, F. Chauvet, M. Arnold, K. Keddadouche and G. Aumaître for their help during chemistry and measurements at CEREGE. We thank D. Lequin (BRGM) for GPS data collection. R.S. Anderson acknowledges support from the University of Colorado College of Arts and Sciences fellowship program.

Bibliography

Balco, G., Stone, J.O., Lifton, N.A., and Dunai, T.J., 2008, A complete and easily accessible means of calculating surface exposure ages or erosion rates from Be-10 and Al-26 measurements: Quaternary Geochronology, v. 3, no. 3, p. 174-195.

Braucher, R., Brown, E.T., Bourlès, D.L., and Colin, F., 2003, In situ produced Be-10 measurements at great depths: implications for production rates by fast muons: Earth And Planetary Science Letters, v. 211, no. 3-4, p. 251-258.

Braucher, R., S. Merchel, J. Borgomano, and D. L. Bourlès (2011), Production of cosmogenic radionuclides at great depth: A multi element approach, Earth and Planetary Science Letters, 309(1-2), 1-9, doi:10.1016/j.epsl.2011.06.036.

Brown, E. T., J. M. Edmond, G. M. Raisbeck, F. Yiou, M. D. Kurz, and E. J. Brook (1991), Examination of surface exposure ages of Antarctic moraines using in situ produced 10Be and 26Al, Geochimica and Cosmochimica Acta, 55(8), 2269.

Chmeleff, J., von Blanckenburg, F., Kossert, K., and Jakob, D., 2010, Determination of the Be-10 half-life by multicollector ICP-MS and liquid scintillation counting: Nuclear Instruments & Methods In Physics Research Section B-Beam Interactions With Materials And Atoms, v. 268, no. 2, p. 192-199.

Clark, J.A., Farrell, W.E., and Peltier, W.R., 1978, Global changes in post glacial sea level: a numerical calculation: Quaternary Research, v. 9, p. 265-287.

Costa, S., Delahaye, D., Freiré-Diaz, S., Davidson, R., Di Nocera, L., and Plessis, E., 2004, Quantification of the Normandy and Picardy chalk cliff retreat by photogrammetric analysis, *dans* Coastal Chalk Cliff Instability, Geological Society, London, Engineering Geology special Publication, p. 139-148.

Devillers, B., Excoffon, P., Morhange, C., Bonnet, S., and Bertoncello, F., 2007, Relative sea-level changes and coastal evolution at Forum Julii (Fréjus, Provence): Comptes Rendus Geosciences, v. 339, no. 5, p. 329-336, doi: 16/j.crte.2007.03.004.

Dornbusch, U., and Robinson, D.A., 2011, Block removal and step backwearing as erosion processes on rock shore platforms: a preliminary case study of the chalk shore platforms of south-east England: Earth Surface Processes and Landforms, v. 36, no. 5, p. 661-671, doi: 10.1002/esp.2086.

Dornbusch, U., Robinson, D.A., Williams, R.B.G., and Moses, C.A., 2007, Chalk shore platform erosion in the vicinity of sea defence structures and the impact of construction methods: Coastal Engineering, v. 54, no. 11, p. 801-810.

Dornbusch, U., Robinson, D.A., Moses, C., Williams, R., and Costa, S., 2006, Chalk cliff retreat in East Sussex and Kent 1870s to 2001: Journal of Maps,, p. 71-78.

Duperret, A., Genter, A., Martinez, A., and Mortimore, R.N., 2004, Coastal chalk cliff instability in NW France: role of lithology, fracture pattern and rainfall, *dans* Coastal Chalk Cliff Instability, Geological Society Engineering Geology Special Publication, London, p. 33-55.

Duperret, A., Taibi, S., Mortimore, R.N., and Daigneault, M., 2005, Effect of groundwater and sea weathering cycles on the strength of chalk rock from unstable coastal cliffs of NW France: Engineering Geology, v. 78, no. 3-4, p. 321.

Edwards, R.J., 2001, Mid- to late holocene relative sea-level change in Poole Harbour, southern England: Journal Of Quaternary Science, v. 16, no. 3, p. 221-235.

Edwards, R.J., 2006, Mid- to late-Holocene relative sea-level change in southwest Britain and the influence of sediment compaction: Holocene, v. 16, no. 4, p. 575-587.

Edwards, R.J., and Horton, B.P., 2000, Reconstructing relative sea-level change using UK salt-marsh foraminifera: Marine Geology, v. 169, no. 1-2, p. 41-56.

Emery, K.O., and Kuhn, G.G., 1982, Sea cliffs: Their processes, profiles and classification: Geological Society of America Bulletin, v. 93, p. 644-654.

Foote, Y., E. Plessis, D. A. Robinson, A. Hénaff, and S. Costa, 2006: Rates and patterns of downwearing of chalk shore platforms of the Channel: comparisons between France and England, in: European Shore Platform Dynamics, D. A. Robinson and Y. Lageat, Eds. Zeitschrift für Geomorphology supplementary volume 144 , p. 93-115.

Gosse, J.C., and Phillips, F.M., 2001, Terrestrial in situ cosmogenic nuclides: theory and application: Quaternary Science Reviews, v. 20, no. 14, p. 1475-1560.

Heisinger, B., D. Lal, A. J. . Jull, P. Kubik, S. Ivy-Ochs, S. Neumaier, K. Knie, V. Lazarev, and E. Nolte, 2002a, Production of selected cosmogenic radionuclides by muons: 1. Fast muons, Earth and Planetary Science Letters, 200(3-4), 345-355, doi:10.1016/S0012-821X(02)00640-4.

Heisinger, B., D. Lal, A. J. T. Jull, P. Kubik, S. Ivy-Ochs, K. Knie, and E. Nolte, 2002b, Production of selected cosmogenic radionuclides by muons: 2. Capture of negative muons, Earth and Planetary Science Letters, 200(3-4), 357-369, doi:10.1016/S0012-821X(02)00641-6.

Hutchinson, J.N., 2002, Chalk flows from the coastal cliffs of northwest Europe, *dans* Catastrophic landslides: Effects, occurrence, and mechanisms, Geological Society of America Reviews in Engineering Geology, Evans S.G. and De Graff J.V., Boulder, Colorado, p. 257-302.

Kanyaya, J.I., and Trenhaile, A.S., 2005, Tidal wetting and drying on shore platforms: An experimental assessment: Geomorphology, v. 70, no. 1-2, p. 129.

Kayanne, H., Ishii, T., Matsumoto, E., and Yonekura, N., 1993, Late Holocene Sea-Level Change on Rota and Guam, Mariana Islands, and Its Constraint on Geophysical Predictions: Quaternary Research, v. 40, no. 2, p. 189-200, doi: 06/qres.1993.1071.

Kiden, P., Denys, L., and Johnston, P., 2002, Late Quaternary sea-level change and isostatic and tectonic land movements along the Belgian-Dutch North Sea coast: geological data and model results: Journal of Quaternary Science, v. 17, no. 5-6, p. 535-546, doi: 10.1002/jqs.709.

Kim, K.J., and Englert, P.A.J., 2004, In situ cosmogenic nuclide production of Be-10 and Al-26 in marine terraces, Fiordland, New Zealand: Nuclear Instruments & Methods In Physics Research Section B-Beam Interactions With Materials And Atoms, v. 223-24, p. 639-644.

Korschinek, G., Bergmaier, A., Faestermann, T., Gerstmann, U.C., Knie, K., Rugel, G., Wallner, A., Dillmann, I., Dollinger, G., and von Gostomski, C.L., 2010, A new value for the half-life of 10Be by Heavy-Ion Elastic Recoil Detection and liquid scintillation counting: Nuclear Instruments and Methods in Physics Research Section B: Beam Interactions with Materials and Atoms, v. 268, no. 2, p. 187-191, doi: 10.1016/j.nimb.2009.09.020.

Lambeck, K., 1997, Sea-Level change along the French Atlantic and Channel coasts since the time of the Last Glacial Maximum: Palaeogeog. Palaeoclim. Palaeoecol., v. 129, p. 1-22.

Lambeck, K., Johnston, P., and Nakada, M., 1990, Holocene glacial rebound and sea-level change in NW Europe: Geophys. J. Int., v. 103, p. 451-468.

de Lange, W.P., and Moon, V.G., 2005, Estimating long-term cliff recession rates from shore platform widths: Engineering Geology, v. 80, no. 3-4, p. 292.

Lasseur, E., Guillocheau, F., Robin, C., Hanot, F., Vaslet, D., Coueffe, R., and Neraudeau, D., 2009, A relative water-depth model for the Normandy Chalk (Cenomanian–Middle Coniacian, Paris Basin, France) based on facies patterns of metre-scale cycles: Sedimentary Geology, v. 213, no. 1-2, p. 1-26, doi: 10.1016/j.sedgeo.2008.10.007.

Massey, A.C., Gehrels, W.R., Charman, D.J., Milne, G.A., Peltier, W.R., Lambeck, K., and Selby, K.A., 2008, Relative sea□level change and postglacial isostatic adjustment along the coast of south Devon, United Kingdom: Journal of Quaternary Science, v. 23, no. 5, p. 415-433, doi: 10.1002/jqs.1149.

Merchel, S., and U. Herpers (1999), An update on Radiochemical Separation Techniques for the Determination of Long-Lived Radionuclides via Accelerator Mass Spectrometry, Radiochimica Acta, 84, 215-219.

Moore, L.J., and Griggs, G.B., 2002, Long-term cliff retreat and erosion hotspots along the central shores of the Monterey Bay National Marine Sanctuary: Marine Geology, v. 181, p. 265-283.

Morhange, C., Laborel, J., and Hesnard, A., 2001, Changes of relative sea level during the past 5000 years in the ancient harbor of Marseilles, Southern France: Palaeogeography, Palaeoclimatology, Palaeoecology, v. 166, no. 3-4, p. 319-329, doi: 16/S0031-0182(00)00215-7.

Mortimore, R.N., Lawrence, J., Pope, D., Duperret, A., and Genter, A., 2004, Coastal cliff geohazards in weak rock: the UK Chalk cliffs of Sussex, *dans* Coastal Chalk Cliff Instability, Geological Society, London, Engineering Geology special Publication, p. 3-31.

Nesteroff, W.D., and Mélières, F., 1967, L'érosion littorale du pays de Caux: Bull Soc. Géol. Fr., v. 7, p. 159-169.

Peltier, W.R., Shennan, I., Drummond, R., and Horton, B., 2002, On the postglacial isostatic adjustment of the British Isles and the shallow viscoelastic structure of the Earth: Geophysical Journal International, v. 148, no. 3, p. 443-475.

Recorbet, F., Rochette, P., Braucher, R., Bourles, D., Benedetti, L., Hantz, D., and Finkel, R.C., 2010, Evidence for active retreat of a coastal cliff between 3.5 and 12 ka in Cassis (South East France): Geomorphology, v. 115, no. 1-2, p. 1-10.

Le Roux, O., Schwartz, S., Gamond, J.F., Jongmans, D., Bourles, D., Braucher, R., Mahaney, W., Carcaillet, J., and Leanni, L., 2009, CRE dating on the head scarp of a major landslide (Sechilienne, French Alps), age constraints on Holocene kinematics: Earth And Planetary Science Letters, v. 280, no. 1-4, p. 236-245.

Siddall, M., Chappell, J., and Potter, E.-K., 2006, Eustatic Sea Level During Past Interglacials, *dans* The climate of past interglacials, Elsevier, Amsterdam, p. 75-92.

Smith, D.E., Cullingford, R.A., Mighall, T.M., Jordan, J.T., and Fretwell, P.T., 2007, Holocene relative sea level changes in a glacio-isostatic area: New data from south-west Scotland, United Kingdom: Marine Geology, v. 242, no. 1-3, p. 5-26, doi: 16/j.margeo.2006.09.015.

Stephenson, W.J., and Kirk, R.M., 2000a, Development of shore platforms on Kaikoura Peninsula, South Island, New Zealand - II: The role of subaerial weathering: Geomorphology, v. 32, no. 1-2, p. 43-56.

Stephenson, W.J., and Kirk, R.M., 2000b, Development of shore platforms on Kaikoura Peninsula, South Island, New Zealand - Part one: The role of waves: Geomorphology, v. 32, no. 1-2, p. 21-41.

Sunamura, T., 1992, Geomorphology of Rocky Coasts: John Wiley & Sons, Chichester, UK.

Trenhaile, A.S., and Byrne, M.-L., 1986, A Theoretical Investigation of the Holocene Development of Rock coasts, with Particular Reference to Shore Platforms: Geografiska Annaler, v. 68 A, no. (1-2), p. 1-14.

Uehara, K., J. D. Scourse, K. J. Horsburgh, K. Lambeck, and A. P. Purcell (2006), Tidal evolution of the northwest European shelf seas from the Last Glacial Maximum to the present, Journal of Geophysical Research, 111, doi:10.1029/2006JC003531.

Waller, M.P., and Long, A.J., 2003, Holocene coastal evolution and sea-level change on the southern coast of England: a review: Journal Of Quaternary Science, v. 18, no. 3-4, p. 351-35